

Object-ABN: Learning to Generate Sharp Attention Maps for Action Recognition

Tomoya Nitta
Nagoya Institute of Technology
Nagoya, Japan

Tsubasa Hirakawa, Hironobu Fujiyoshi
Chubu University, Aichi, Japan

Toru Tamaki
Nagoya Institute of Technology
Nagoya, Japan

Abstract

In this paper we propose an extension of the Attention Branch Network (ABN) by using instance segmentation for generating sharper attention maps for action recognition. Methods for visual explanation such as Grad-CAM usually generate blurry maps which are not intuitive for humans to understand, particularly in recognizing actions of people in videos. Our proposed method, Object-ABN, tackles this issue by introducing a new mask loss that makes the generated attention maps close to the instance segmentation result. Further the PC loss and multiple attention maps are introduced to enhance the sharpness of the maps and improve the performance of classification. Experimental results with UCF101 and SSv2 shows that the generated maps by the proposed method are much clearer qualitatively and quantitatively than those of the original ABN.

1. Introduction

Action recognition [20, 24, 36, 45, 53] is one of long-standing topics in computer vision and still actively studied thanks to the emergence of deep learning techniques and large datasets. The task is to classify a trimmed video clip (typically several second-long) into pre-defined action categories [8, 9]. It is a basis of other video-related tasks such as temporal action localization [47] where untrimmed videos are divided into short clips whose features are extracted by using action recognition models.

Deep models, not limited to action recognition but also other tasks, are difficult to investigate because of its black-box nature, hence visual explanations have been studied in the field of explainable AI [1, 7, 19, 31, 35, 44]. These are attempts to generate saliency maps to visualize which of the parts in the scene are important for classification, and

many methods have been utilized, including Grad-CAM [37], Score-CAM [46], LRP [3], and ABN [11]. A common problem of these approaches is that generated maps are often blurry and ambiguous, hence difficult to understand and interpret for human observers [1, 17]. Recent studies have therefore been attempting to improve the quality and sharpness of the maps by focusing on objects, for example, by combining Grad-CAM and LRP [25], applying LRP to Vision Transformers [5], improving ABN with Score-CAM [26], and even human intervention [33] or additional supervision [27].

For action recognition, this blurry map issue still remains while many visual explanation methods tailored for videos have been proposed. The challenge is to make the model focus on the regions of people who perform the actions in the scene. To this end, some works evaluate visualization results by checking the peak of the map being inside bounding boxes of humans (called pointing games) [4, 29, 30, 50, 51]. However, this is not a direct approach to the blurry map issue, and models still suffer from from the representation bias; models may use clues of backgrounds of the scene instead of the foreground [16, 28, 53].

In this paper, we propose *Object-ABN*, a direct and simple approach to the blurry map issue of action recognition. The key idea is to combine an off-the-shelf instance segmentation model with Attention Branch Network (ABN) [11] (Fig.1(a)). ABN is a classification model with attention and perception branches; the attention branch generates an attention map and uses it as weights of the feature map fed to the perception branch. The attention branch has its own classifier to improve the predictive power of the attention map. In the proposed method (Fig.1(b)), a constraint is added so that the attention map is close to the instance segmentation result. This is expected to lead to a better explainability with a sharper map focusing on people and objects in the scene. However, a possible drawback is the

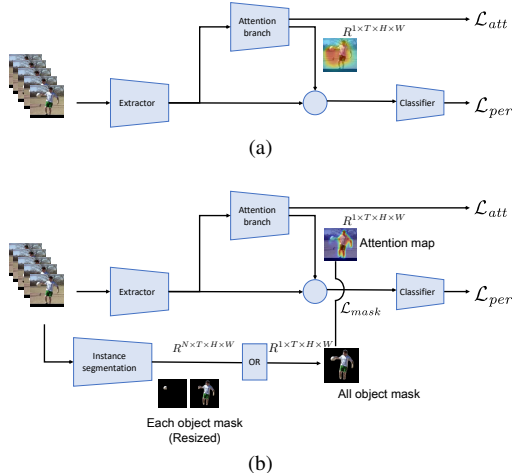


Figure 1. Overview of models of (a) ABN for action recognition, and (b) the proposed Object-ABN.

performance-explainability trade-off when adding explanation modules to a model [1, 7, 31, 35]. To mitigate this, we propose to use Prototype Conformity (PC) loss [34] that enforces features to be separated in several clusters. In the following sections, we summarize related works, and we briefly describe ABN, then explain the proposed Object-ABN in detail. Then we show experimental results with two datasets, UCF101 [41] and Something-Something v2 [14], with quantitative evaluation on the sharpness of attention maps.

2. Related works

Explainable AI (XAI) [1, 7, 19, 31, 35, 44] has become an important topic particularly for deep learning models. Visual explanation (or visual attribution) is a topic of XAI, which is to generate a map (sometimes called saliency map, attention map, or attribution map) that visually indicates where in the image the model is focusing on for classification.

Methods are often categorized into post-hoc and intrinsic [1, 7, 19, 31, 35, 44]. *Post-hoc* methods are used to analyse a single prediction of a trained model, and the name comes from the fact that the visual explanation is done after the model has been trained and fixed. This category includes well-known methods such as CAM [52], Grad-CAM [37], and LRP [3]. These were originally proposed for images, but can be used for videos as well, so they have been used as a baseline for comparison. In addition, some works proposed post-hoc methods tailored for videos by extending methods for images. For example, DevNet [12] used gradient-based Deep Inside CNN [40] and graph-cut for extracting important regions, EB-RNN [4] is based on Excitation Backprop (EB) [50, 51] for models with CNN and RNN,

and EP-3D and ST-EP [29, 30] extends Extremal Perturbation (EP) [10] for spatio-temporal 3D volumes. LRP/DTD [3] has also been applied to videos [2, 18]. Few methods have been proposed specific for video; saliency tubes [43] proposed an additional module for visualizing spatio-temporal tubes, and class feature pyramids [42] proposed a feature back-propagation of 3D CNN.

The post-hoc approach is useful for investigating the behavior of a given model, particularly sensitively can be visualized by showing maps for each category. However, post-hoc methods based on gradients (Grad-CAM [37]) and back-propagation (LRP [3]) are inherently difficult to generate sharp maps because class-prediction information flows from the top to the bottom through the network. Therefore some attempts have been proposed to make the map sharper; for example, Relevance-CAM [25] combines LRP and Grad-CAM. Perturbation-based methods [10, 50] suffer from the same problem, as well as a high computation cost for perturbing masks many times for video volumes.

Intrinsic methods has its own mechanism of visual explanation in the model itself. This approach has an advantage that the model is designed to have explainability in the first place [35], and that visual explanation during a training phase would be useful for practitioners to check the model performance qualitatively. Because the explanation mechanism of an intrinsic method is a part of the model, there are a great variety of model architectures. Sharma *et al.* [38, 39] used LSTM to predict the soft attention map of the next frame, which were later extended to video captioning with attention [48]. Attention pooling [13] decomposed a 3D attention map with 2nd order pooling and rank-1 approximation. Interpretable spatio-temporal attention [32] used spatial and temporal attention via ConvLSTM. Recent self-attention mechanisms are also introduced in STA-TSN [49] and GTA [15], as well as Transformer-based video models [36]. Some of these methods do not aim to visual explanation, and the blurry map issue still remains for videos because the ability of temporal modeling, which is useful for classification, may be harmful to capture sharp spatial attention maps.

In this paper, we focus on ABN [11], an intrinsic method proposed for images. ABN first extracts features, then the attention branch computes an attention map which is multiplied to the feature map, then the perception branch classifies the weighted feature map (see Fig.1(a)). The attention map of ABN is useful as visual explanation because the attention map directly specifies the importance of the feature map that is used for classification. However, sometimes the attention map of ABN differs greatly from the human intuition. To alleviate this problem, a Human-in-the-loop (HITL) framework [21] was proposed to enable human operators to modify the attention map of ABN. This results in a sharper attention map that are easy to interpret by humans,

leading to a better explainability through attention visualization. However, human intervention on videos that requires frame-by-frame annotations is costly and impractical. In contrast, our proposed Object-ABN scales to a large amount of video frames because it is trained in an end-to-end manner by introducing instance segmentation as an additional self-supervision.

3. Method

In this section, we describe ABN [11] for action recognition. Although the original ABN was proposed for classifying images, notations are aligned with the the proposed models described below.

3.1. ABN

ABN consists of feature extractor E , attention branch A , and perception branch P . Let input video clip be $x \in \mathbb{R}^{T_{in} \times 3 \times H_{in} \times W_{in}}$, where T_{in} is the number of video frames, H_{in}, W_{in} are height and width of the frame. The corresponding ground-truth action label is denoted by $y \in \{0, 1\}^L$, where L is the number of categories.

First, the extractor takes a video clip and output feature maps $h_1 = E(x) \in \mathbb{R}^{T \times C \times H \times W}$, where C is the channel size. Then the attention branch takes it and generates frame-wise (unconstrained) attention maps $M_u \in [0, 1]^{T \times 1 \times H \times W}$ and class prediction $y_a \in [0, 1]^L$ as well. The maps M_u are applied to feature maps h_1 of each frame separately to generate $h_2 \in \mathbb{R}^{T \times C \times H \times W}$ as

$$h_{2,t,c} = h_{1,t,c} M_{u,t}, \text{ for } t = 1, \dots, T \text{ } c = 1, \dots, C. \quad (1)$$

The loss attached to the attention branch is $\mathcal{L}_{att} = \mathcal{L}_{CE}(y_a, y)$, where \mathcal{L}_{CE} is a cross entropy loss.

The perception branch P takes weighted feature maps h_2 and outputs prediction $y_p = P(h_2) \in [0, 1]^L$. The loss of this branch is $\mathcal{L}_{per} = \mathcal{L}_{CE}(y_p, y)$.

3.2. Object-ABN

As mentioned before, the attention maps M_u generated by ABN is blurry and often different from areas where people consider important. In this study, we assume that regions of people and objects in the scene are important for identifying action categories, and we enforce on the shape of the attention map being closer to the scene objects. We call this Object-ABN.

To this end, we propose to apply a pre-trained instance segmentation model to each frame of the video clip, which generates the ground-truth object masks $M_{gt} \in \{0, 1\}^{T \times N(t) \times H \times W}$ for instances that appear in the video clip. $N(t)$ is the number of instances detected at frame t , so it differs at different frames. We aggregate the object masks to a single channel mask $M'_{gt} \in \{0, 1\}^{T \times 1 \times H \times W}$ by using

logical OR as follows;

$$M'_{gt,t} = \bigcup_{c=1}^{N(t)} M_{gt,t,c}. \quad (2)$$

This is used to compute the following mask loss

$$\mathcal{L}_{mask} = \mathcal{L}_{MSE}(M_o, M'_{gt}), \quad (3)$$

which is a mean squared error (MSE) loss between the ground-truth object masks and the attention maps M_o . Here we use M_o as the ABN attention maps (instead of M_u) to show that it is constrained by the object masks M'_{gt} .

3.3. Using multiple attention maps

Object-ABN generates the object-constrained attention maps M_o for each frame t , that is, $M_{o,t}$ for $t = 1, \dots, T$. Each map has a single channel, which means that the same attention map is applied to all C channels of features h_1 . However, different channels of h_1 may capture different concepts of the scene, and it might be desirable to use different attention maps for different channels.

Therefore, in this study, we propose to use multiple attention maps by using multi-head attention (MHA). Specifically, we use C' heads to output maps in the attention branch, and each head c' generates attention maps $M_{c'} \in [0, 1]^{T \times 1 \times H \times W}$.

The number of heads C' can be different from the number of channels C , and we align the dimensions as follows. First, we apply the attention map $M_{c'}$ to each channel c of h_1 ;

$$h_{1,t,c}^{c'} = h_{1,t,c} M_{c',t} \in \mathbb{R}^{T \times C \times H \times W}, \quad (4)$$

then concatenate them in the channel direction;

$$h'_1 = \text{cat}(h_1^1, h_1^2, \dots, h_1^{C'}) \in \mathbb{R}^{T \times (CC') \times H \times W}, \quad (5)$$

and use a 1×1 convolution

$$h_2 = \text{conv}(h'_1) \in \mathbb{R}^{T \times C \times H \times W}, \quad (6)$$

with the kernel size of $1 \times (CC') \times 1 \times 1$ to generate h_2 with the appropriate dimension.

In this study, we set $C' = 3$. This means there are three attention maps M_1, M_2 , and M_3 , and we denote them as M_u, M_o , and M_b , respectively. M_u is the unconstrained attention maps as in the original ABN, and M_o is the object-constrained map M_o of Object-ABN. M_b is the attention maps of the background. In action recognition, it is known that the background can be a clue for classification [16, 53] because of the representation bias [28]. We use two maps for foreground and background by explicitly separating them.

We introduce the following loss for three attention maps;

$$\mathcal{L}_{mha} = \mathcal{L}_{\text{MSE}}(M_o, M'_{gt}) + \lambda_b \mathcal{L}_{\text{MSE}}(M_b, 1 - M'_{gt}), \quad (7)$$

where λ_b is a weight. The first term is the same with the mask loss (3). The second term is for the background attention maps M_b and uses the inverse of the ground-truth object masks. Note that we don't use any losses for M_u , and let the network to obtain the map by itself because the unconstrained maps might be useful like as in the original ABN.

3.4. PC Loss

When creating attention maps, it would be desirable to have features well separated in the middle of the network, particularly in the attention branch, because the attention branch can generate maps suitable for each action categories. To this end, we introduce the Prototype Conformity (PC) loss [34], which encourages cluster to be generated in the latent space and facilitates feature separation. The use of clustered features would be advantageous for generating sharp attention maps while preserving accuracy.

We use the PC loss for features $f \in R^d$ in the attention branch. The loss is represented by

$$\begin{aligned} \mathcal{L}_{PC} = & \lambda_{PC_1} \|f - w_y^c\|_2 \\ & - \frac{\lambda_{PC_2}}{K-1} \sum_{j \neq y} (\|f - w_j^c\|_2 + \|w_y^c - w_j^c\|_2), \end{aligned} \quad (8)$$

where y is the label, K is the number of clusters, and w_j^c is the j -th trainable centroid.

The total loss is one of the following;

$$\mathcal{L} = \mathcal{L}_{per} + \lambda \mathcal{L}_{att} + \lambda_{mask} \mathcal{L}_{mask} + \lambda_{PC} \mathcal{L}_{PC} \quad (9)$$

$$\mathcal{L} = \mathcal{L}_{per} + \lambda \mathcal{L}_{att} + \lambda_{mha} \mathcal{L}_{mha} + \lambda_{PC} \mathcal{L}_{PC}, \quad (10)$$

where λ , λ_{mask} , λ_{mha} , and λ_{PC} are weights.

4. Experiment

4.1. Datasets

We used two datasets in the experiments; UCF101 [41], and something-something v2 (SSv2) [14].

UCF101 [41] has 101 classes of human actions, consisting of a training set of about 9500 videos and a validation set of about 3500 videos. Each video was collected from Youtube, with an average length of 7.21 seconds. We report the performance of the first split.

SSv2 [14] consists of a training set of 168913 videos, a validation set of 24777 videos. Each video is about 2 to 6 second-long (average 4.03 seconds), filmed by a crowd worker. The video contains 173 different templates as action categories, such as "Dropping [something] into [something]" that represents the action performed on objects.

4.2. Experimental setting

Training. From a video in the training set, we sampled 16 frames with a stride of four frames (starting at randomly decided frame) to make an input clip. We resized the shorter side of the frame randomly in the range of 256 to 320 pixels while keeping the aspect ratio, randomly cropped a square of size 224×224 pixels, and then performed the horizontal flip with a probability of 50%. The optimizer used for training was Adam [23] with the learning rate of 10^{-4} , and the number of training epochs was set to 50.

Validation. We sampled one clip is sampled from a video in the validation set as in the training, and resized the short side to 256 pixels while maintaining the aspect ratio, then cropped the square patch of size 224×224 pixels in the center of the frame.

Evaluating sharpness. For a quantitative evaluation of the sharpness of attention maps, we propose to use entropy of the maps. If the attention maps are blurry across the entire frames, the distribution of values of the maps becomes broad and the entropy increases. If the attention maps are sharp, the distribution should be polarized toward 0 and 1, entropy should decrease, and the boundary between people and background is expected to be sharper. Therefore, we use the entropy as an indicator of the sharpness the attention maps. However, the entropy decreases when the attention maps are flat and values falls within a certain range. To mitigate this, we normalize the attention map at each frame so that the minimum and maximum values of maps are 0 and 1, respectively.

To compute the entropy, we create a histogram of attention maps with $N = 10$ bins from 0 to 1. The frequency $hist[i]$ of each bin i of the histogram is the normalized discrete probability p_i , which is used to compute the entropy as follows;

$$\text{entropy} = \sum_{i=1}^N -p_i \log_2 p_i, \quad p_i = \frac{hist[i]}{\sum_{j=1}^N hist[j]}. \quad (11)$$

The entropy is calculated for each frame of the video clip, and the entropy of the video is calculated by averaging the entropy of all frames.

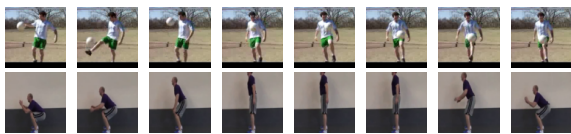
As a reference, the maximum of the entropy is achieved when values are $p_i = 1/N$. Since $N = 10$ in our case, $\log_2 10 \approx 3.332$ is the maximum value.

Model. As a backbone of ABN, we used X3D-M [8] pre-trained on Kinetics400 [22]. We divided the X3D-M model in two between the third and fourth ResBlocks, using the first half as the feature extractor and the second half as the perception branch. We added an attention branch comprising of three ResBlocks and two conv layers, and the features immediately after the three ResBlocks were used to compute the PC loss.

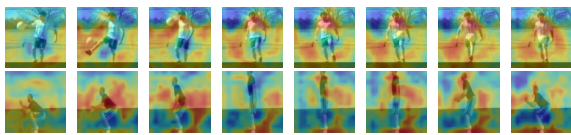
The resulting model takes an input video clip of size

Table 1. The performances and entropy values with different configurations for the validation set of UCF101.

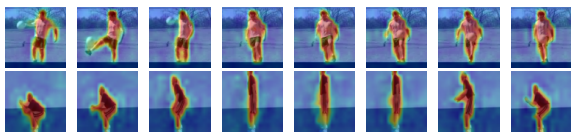
$\mathcal{L}_{per/attn}$	\mathcal{L}_{mask}	\mathcal{L}_{mha}	\mathcal{L}_{PC}	entropy				
				top-1	top-5	M_u	M_o	M_b
✓				93.96	99.15	3.064		
✓			✓	94.68	99.47	3.041		
✓	✓			93.62	99.26		2.026	
✓	✓		✓	93.80	98.97		1.469	
✓		✓		88.93	98.04	2.850	1.360	1.356
✓		✓	✓	87.76	97.27	2.815	1.388	1.414
interpretable attention [32]				87.11				
STA-TSN [49] RGB				83.4				
STA-TSN [49] RGB+flow				92.8				
ST-SAWVLAD [6]				94.8				



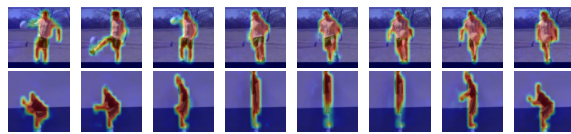
(a)



(b) M_u with $\mathcal{L}_{per/attn}$



(c) M_o with $\mathcal{L}_{per/attn} + \mathcal{L}_{mask}$

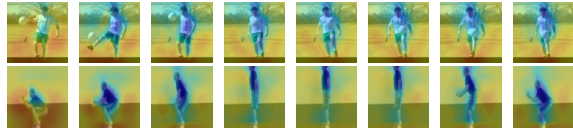


(d) M_o with $\mathcal{L}_{per/attn} + \mathcal{L}_{mask} + \mathcal{L}_{PC}$

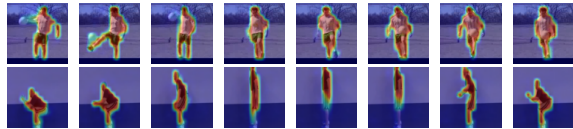
Figure 2. Visualization of results for the validation set of UCF101. (a) Input videos (every two frames out of 16 frames of a clip are shown). (b) Unconstrained maps M_u with $\mathcal{L}_{per/attn}$ (original ABN). (c) Object-constrained maps M_o with $\mathcal{L}_{per/attn}$, and \mathcal{L}_{mask} , as well as (d) \mathcal{L}_{PC} .

$T_{in} \times H_{in} \times W_{in} = 16 \times 244 \times 244$, and generates an attention map of size $T \times H \times W = 16 \times 14 \times 14$ which is the spatial resolution of the third ResBlock of the X3D-M.

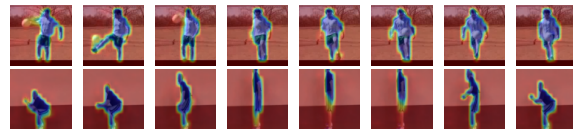
Parameters. The parameters used in the experiment were set as follows; $\lambda = 1$, $\lambda_b = 1$, $\lambda_{mask} = 10$, $\lambda_{mha} = 10$, $\lambda_{PC} = 10^{-4}$, $\lambda_{PC_1} = 1$, and $\lambda_{PC_2} = 10^{-3}$. The number of clusters K was set to L , the number of categories.



(a) M_u with $\mathcal{L}_{per/attn}$ and \mathcal{L}_{mha}



(b) M_o with $\mathcal{L}_{per/attn}$ and \mathcal{L}_{mha}



(c) M_b with $\mathcal{L}_{per/attn}$ and \mathcal{L}_{mha}

Figure 3. Visualization of results for the validation set of UCF101 with $\mathcal{L}_{per/attn}$ and \mathcal{L}_{mha} . Three types of maps (a) M_u , (b) M_o , and (c) M_b .

4.3. Experimental results for UCF101

We obtained main results with UCF101, which are shown in Tab.1. Each row shows the performance and entropy with different configurations of losses. The first row with $\mathcal{L}_{per/attn}$ only is equivalent to the original ABN, and the second rows is the original ABN with the PC loss \mathcal{L}_{PC} . In the following rows, results are of Object-ABN with either of \mathcal{L}_{mask} and \mathcal{L}_{mha} is used, and with or without the PC loss.

4.3.1 Mask loss

First, we compare the original ABN with the proposed Object-ABN to verify the effect of the mask loss. As can be seen from the first row ($\mathcal{L}_{per/attn}$ only) and third row ($\mathcal{L}_{per/attn}$ and \mathcal{L}_{mask}) of Tab.1, the difference in the top-1 performance is 0.3 and not so large. However, the entropy decreased by more than 1 when the mask loss is used, which means that quantitatively the sharpness of the attention map was drastically improved.

Also, the generated attention maps are completely different. In case of using the mask loss (Fig.2(c)), generated maps M_o are sharp so that objects and people are clearly visible, while the case without the mask loss (Fig.2(b)) produced maps M_u that are blurry and speckled, and action-related foreground and background doesn't appear.

4.3.2 PC Loss

Next, we see how the PC loss affect the performance and the attention maps. As shown in Tab.1, using the PC loss

reduces the entropy values and improve the performances for the cases with the original ABN (the first two rows) and Object-ABN with \mathcal{L}_{mask} (the two middle rows). However, when \mathcal{L}_{mha} is used, the PC loss seems not to contribute the improvements.

Figures 2(d) shows maps with the PC loss. Compared with Fig.2(c) without the PC loss, the separation of the background and foreground is clearer, and the fluctuations in the background disappear.

4.3.3 Multiple attention maps

Here, we shows the effect of multi-head attention maps. Corresponding results are the last two rows of Tab.1, where the performance dropped by about 5 % compared to the cases without \mathcal{L}_{mha} , even with the PC loss. Hence, in terms of performance, using a single attention map would be better.

However the entropy values becomes smaller and the quality of the maps were further improved by using \mathcal{L}_{mha} , as shown in Fig.3. The object-constrained mask M_o (Fig.3(b)) are far more sharper than those with \mathcal{L}_{mask} (Fig.2(c)), and even with \mathcal{L}_{PC} (Fig.2(d)).

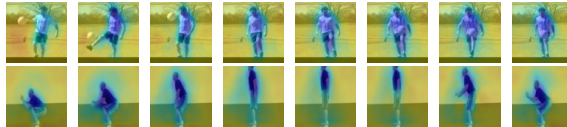
4.3.4 Comparisons with other methods

Table 1 also shows performances of other methods that are intrinsic models for action recognition for the purpose of visualizing attention maps. Of course none of them have published entropy values, however their results are visually much worse than our results in terms of the sharpens of the attention maps. The performances of our method are comparable or better,

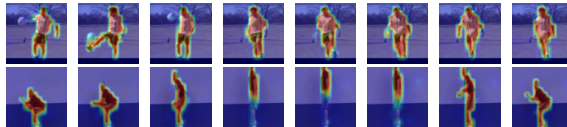
4.4. Experimental result for SSv2

Here we show the experimental results for SSv2. The training settings was the same with UCF101, except for the frame sampling stride (two frames instead of four), no horizontal flip, and 25 epochs for training. Performances are shown in Tab.2, and visualization results with the mask loss are shown in Fig.5, and with the multiple attention maps in Fig.6.

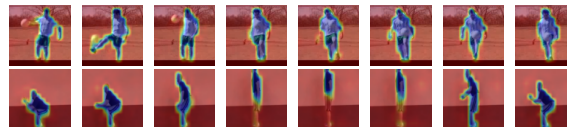
The performance was improved from the original ABN by adding the mask loss, and the entropy of M_o for the Object-ABN is smaller than that of M_u for ABN. Furthermore, using the PC loss and adding the multiple attention maps improve the performance. The object-constrained maps M_o shown in Fig.5(c)(d) and Fig.6(b) look almost the same, supported by the similar entropy values in Tab.2. This suggests that for this dataset the mask loss has the largest impact on the sharpness of the maps, while the multiple attention maps and the PC loss also contribute to the performance.



(a) M_u with $\mathcal{L}_{per/attn} + \mathcal{L}_{mha} + \mathcal{L}_{PC}$



(b) M_o with $\mathcal{L}_{per/attn} + \mathcal{L}_{mha} + \mathcal{L}_{PC}$



(c) M_b with $\mathcal{L}_{per/attn} + \mathcal{L}_{mha} + \mathcal{L}_{PC}$

Figure 4. Visualization of results for the validation set of UCF101 with $\mathcal{L}_{per/attn}$, \mathcal{L}_{mha} , and \mathcal{L}_{PC} . Three types of maps (a) M_u , (b) M_o , and (c) M_b .

Table 2. The performances and entropy values with different configurations for the validation set of SSv2.

$\mathcal{L}_{per/attn}$	\mathcal{L}_{mask}	\mathcal{L}_{mha}	\mathcal{L}_{PC}	entropy				
				top-1	top-5	M_u	M_o	M_b
✓				54.63	83.23	2.887		
✓	✓			54.83	82.73		2.331	
✓		✓	✓	54.97	83.15		2.427	
✓			✓	55.05	83.60	2.921	2.236	2.237

The unconstrained maps M_u are shown in Fig.5(b) for ABN and Fig.6(a) for the proposed method. For the maps of ABN, the attentions to the object and hands are weaker (in blue) than to the background at the beginning. After the action starts, the attention is getting focused on the object, then becomes strong at the end. In contrast, the maps of the proposed method are flat at first, then the attention is continuously focused on the object during the action until the end. Therefore, the maps of the proposed method are expected to better represent the temporal information of the action.

5. Conclusion

In this paper, we have proposed Object-ABN, an extension of ABN by using instance segmentation, and enables the generation of sharper attention maps, which enable us to clearly see which parts of the scene the model is focusing on. Experiments with two datasets demonstrated that the proposed method with the mask loss, multiple attention maps, and the PC loss improves the quality of attention maps in terms of entropy, as well as the classification performances.

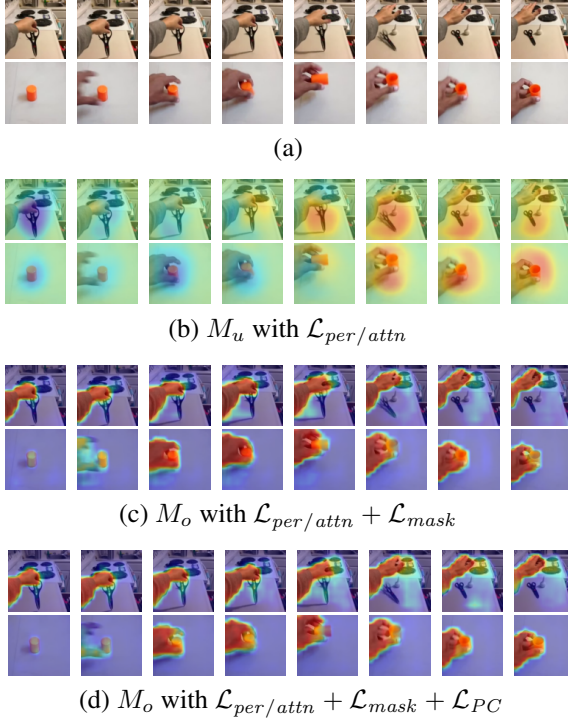


Figure 5. Visualization of results for the validation set of SSv2. (a) Input videos. (b) M_u with $\mathcal{L}_{per/attn}$. (c) M_o with $\mathcal{L}_{per/attn}$, and \mathcal{L}_{mask} , as well as (d) \mathcal{L}_{PC} .

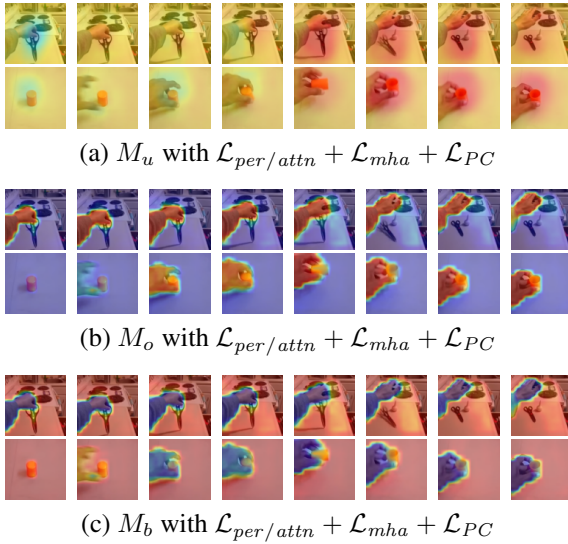


Figure 6. Visualization of results for the validation set of SSv2 with $\mathcal{L}_{per/attn}$, \mathcal{L}_{mha} , and \mathcal{L}_{PC} . Three types of maps (a) M_u , (b) M_o , and (c) M_b .

References

[1] Amina Adadi and Mohammed Berrada. Peeking inside the black-box: A survey on explainable artificial intelligence

(xai). *IEEE Access*, 6:52138–52160, 2018. 1, 2

[2] Christopher J. Anders, Grégoire Montavon, Wojciech Samek, and Klaus-Robert Müller. Understanding patch-based learning of video data by explaining predictions. In Wojciech Samek, Grégoire Montavon, Andrea Vedaldi, Lars Kai Hansen, and Klaus-Robert Müller, editors, *Explainable AI: Interpreting, Explaining and Visualizing Deep Learning*, volume 11700 of *Lecture Notes in Computer Science*, pages 297–309. Springer, 2019. 2

[3] Sebastian Bach, Alexander Binder, Grégoire Montavon, Frederick Klauschen, Klaus-Robert Müller, and Wojciech Samek. On pixel-wise explanations for non-linear classifier decisions by layer-wise relevance propagation. *PLOS ONE*, 10(7):1–46, 07 2015. 1, 2

[4] Sarah Adel Bargal, Andrea Zunino, Donghyun Kim, Jianming Zhang, Vittorio Murino, and Stan Sclaroff. Excitation backprop for rnns. In *2018 IEEE Conference on Computer Vision and Pattern Recognition, CVPR 2018, Salt Lake City, UT, USA, June 18–22, 2018*, pages 1440–1449. Computer Vision Foundation / IEEE Computer Society, 2018. 1, 2

[5] Hila Chefer, Shir Gur, and Lior Wolf. Transformer interpretability beyond attention visualization. In *Proceedings of the IEEE/CVF Conference on Computer Vision and Pattern Recognition (CVPR)*, pages 782–791, June 2021. 1

[6] Shilei Cheng, Mei Xie, Zheng Ma, Siqi Li, Song Gu, and Feng Yang. Spatio-temporal self-attention weighted VLAD neural network for action recognition. *IEICE Trans. Inf. Syst.*, 104-D(1):220–224, 2021. 5

[7] Arun Das and Paul Rad. Opportunities and challenges in explainable artificial intelligence (XAI): A survey. *CoRR*, abs/2006.11371, 2020. 1, 2

[8] Christoph Feichtenhofer. X3d: Expanding architectures for efficient video recognition. In *Proceedings of the IEEE/CVF Conference on Computer Vision and Pattern Recognition (CVPR)*, June 2020. 1, 4

[9] Christoph Feichtenhofer, Haoqi Fan, Jitendra Malik, and Kaiming He. Slowfast networks for video recognition. In *Proceedings of the IEEE/CVF International Conference on Computer Vision (ICCV)*, October 2019. 1

[10] Ruth Fong, Mandela Patrick, and Andrea Vedaldi. Understanding deep networks via extremal perturbations and smooth masks. In *Proceedings of the IEEE/CVF International Conference on Computer Vision (ICCV)*, October 2019. 2

[11] Hiroshi Fukui, Tsubasa Hirakawa, Takayoshi Yamashita, and Hironobu Fujiyoshi. Attention branch network: Learning of attention mechanism for visual explanation. In *Proceedings of the IEEE/CVF Conference on Computer Vision and Pattern Recognition (CVPR)*, June 2019. 1, 2, 3

[12] Chuang Gan, Naiyan Wang, Yi Yang, Dit-Yan Yeung, and Alexander G. Hauptmann. Devnet: A deep event network for multimedia event detection and evidence recounting. In *IEEE Conference on Computer Vision and Pattern Recognition, CVPR 2015, Boston, MA, USA, June 7–12, 2015*, pages 2568–2577. IEEE Computer Society, 2015. 2

[13] Rohit Girdhar and Deva Ramanan. Attentional pooling for action recognition. In I. Guyon, U. V. Luxburg, S. Bengio,

- H. Wallach, R. Fergus, S. Vishwanathan, and R. Garnett, editors, *Advances in Neural Information Processing Systems*, volume 30. Curran Associates, Inc., 2017. 2
- [14] Raghav Goyal, Samira Ebrahimi Kahou, Vincent Michalski, Joanna Materzynska, Susanne Westphal, Heuna Kim, Valentin Haenel, Ingo Fruend, Peter Yianilos, Moritz Mueller-Freitag, Florian Hoppe, Christian Thureau, Ingo Bax, and Roland Memisevic. The "something something" video database for learning and evaluating visual common sense. In *Proceedings of the IEEE International Conference on Computer Vision (ICCV)*, Oct 2017. 2, 4
- [15] Bo He, Xitong Yang, Zuxuan Wu, Hao Chen, Ser-Nam Lim, and Abhinav Shrivastava. Gta: Global temporal attention for video action understanding. In *Proceedings of the British Machine Vision Conference (BMVC)*, November 2021. 2
- [16] Yun He, Soma Shirakabe, Yutaka Satoh, and Hirokatsu Kataoka. Human action recognition without human. *CoRR*, abs/1608.07876, 2016. 1, 3
- [17] Liam Hiley, Alun D. Preece, and Yulia Hicks. Explainable deep learning for video recognition tasks: A framework & recommendations, 2019. 1
- [18] Liam Hiley, Alun D. Preece, Yulia Hicks, A. David Marshall, and Harrison Taylor. Discriminating spatial and temporal relevance in deep taylor decompositions for explainable activity recognition. *CoRR*, abs/1908.01536, 2019. 2
- [19] Xiaowei Huang, Daniel Kroening, Wenjie Ruan, James Sharp, Youcheng Sun, Emese Thamo, Min Wu, and Xinpeng Yi. A survey of safety and trustworthiness of deep neural networks: Verification, testing, adversarial attack and defence, and interpretability. *Computer Science Review*, 37:100270, 2020. 1, 2
- [20] Matthew S. Hutchinson and Vijay N. Gadepally. Video action understanding. *IEEE Access*, 9:134611–134637, 2021. 1
- [21] Takaaki Iwayoshi, Masahiro Mitsuhara, Masayuki Takada, Tsubasa Hirakawa, Takayoshi Yamashita, and Hironobu Fujiyoshi. Attention mining branch for optimizing attention map. In *17th International Conference on Machine Vision and Applications (MVA)*, 2021. 2
- [22] Will Kay, Joao Carreira, Karen Simonyan, Brian Zhang, Chloe Hillier, Sudheendra Vijayanarasimhan, Fabio Viola, Tim Green, Trevor Back, Paul Natsev, Mustafa Suleyman, and Andrew Zisserman. The kinetics human action video dataset, 2017. 4
- [23] Diederik P. Kingma and Jimmy Ba. Adam: A method for stochastic optimization. In Yoshua Bengio and Yann LeCun, editors, *3rd International Conference on Learning Representations, ICLR 2015, San Diego, CA, USA, May 7-9, 2015, Conference Track Proceedings*, 2015. 4
- [24] Yu Kong and Yun Fu. Human action recognition and prediction: A survey. *CoRR*, abs/1806.11230, 2018. 1
- [25] Jeong Ryong Lee, Sewon Kim, Inyong Park, Taejoon Eo, and Dosik Hwang. Relevance-cam: Your model already knows where to look. In *Proceedings of the IEEE/CVF Conference on Computer Vision and Pattern Recognition (CVPR)*, pages 14944–14953, June 2021. 1, 2
- [26] Kwang Hee Lee, Chaewon Park, Jungyun Oh, and Nojun Kwak. Lfi-cam: Learning feature importance for better visual explanation. In *Proceedings of the IEEE/CVF International Conference on Computer Vision (ICCV)*, pages 1355–1363, October 2021. 1
- [27] Kumpeng Li, Ziyang Wu, Kuan-Chuan Peng, Jan Ernst, and Yun Fu. Tell me where to look: Guided attention inference network. In *Proceedings of the IEEE Conference on Computer Vision and Pattern Recognition (CVPR)*, June 2018. 1
- [28] Yingwei Li, Yi Li, and Nuno Vasconcelos. Resound: Towards action recognition without representation bias. In *Proceedings of the European Conference on Computer Vision (ECCV)*, September 2018. 1, 3
- [29] Zhenqiang Li, Weimin Wang, Zuoyue Li, Yifei Huang, and Yoichi Sato. Towards visually explaining video understanding networks with perturbation. In *IEEE Winter Conference on Applications of Computer Vision, WACV 2021, Waikoloa, HI, USA, January 3-8, 2021*, pages 1119–1128. IEEE, 2021. 1, 2
- [30] Zhenqiang Li, Weimin Wang, Zuoyue Li, Yifei Huang, and Yoichi Sato. Spatio-temporal perturbations for video attribution. *IEEE Transactions on Circuits and Systems for Video Technology*, 32(4):2043–2056, 2022. 1, 2
- [31] Pantelis Linardatos, Vasilis Papastefanopoulos, and Sotiris Kotsiantis. Explainable ai: A review of machine learning interpretability methods. *Entropy*, 23(1), 2021. 1, 2
- [32] Lili Meng, Bo Zhao, Bo Chang, Gao Huang, Wei Sun, Frederick Tung, and Leonid Sigal. Interpretable spatio-temporal attention for video action recognition. In *Proceedings of the IEEE/CVF International Conference on Computer Vision (ICCV) Workshops*, Oct 2019. 2, 5
- [33] Masahiro Mitsuhara, Hiroshi Fukui, Yusuke Sakashita, Takanori Ogata, Tsubasa Hirakawa, Takayoshi Yamasita, and Hironobu Fujiyoshi. Embedding human knowledge into deep neural network via attention map. In *International Conference on Computer Vision Theory and Applications (VIS-APP)*, 2021. 1
- [34] Aamir Mustafa, Salman Khan, Munawar Hayat, Roland Goecke, Jianbing Shen, and Ling Shao. Adversarial defense by restricting the hidden space of deep neural networks. In *Proceedings of the IEEE/CVF International Conference on Computer Vision (ICCV)*, October 2019. 2, 4
- [35] Gabrielle Ras, Ning Xie, Marcel van Gerven, and Derek Doran. Explainable deep learning: A field guide for the uninitiated. *Journal of Artificial Intelligence Research*, 73:329–396, feb 2022. 1, 2
- [36] Javier Selva, Anders S. Johansen, Sergio Escalera, Kamal Nasrollahi, Thomas B. Moeslund, and Albert Clapés. Video transformers: A survey. *CoRR*, abs/2201.05991, 2022. 1, 2
- [37] Ramprasaath R. Selvaraju, Michael Cogswell, Abhishek Das, Ramakrishna Vedantam, Devi Parikh, and Dhruv Batra. Grad-cam: Visual explanations from deep networks via gradient-based localization. In *Proceedings of the IEEE International Conference on Computer Vision (ICCV)*, Oct 2017. 1, 2
- [38] Shikhar Sharma, Ryan Kiros, and Ruslan Salakhutdinov. Action recognition using visual attention. *CoRR*, abs/1511.04119, 2015. 2

- [39] Shikhar Sharma, Ryan Kiros, and Ruslan Salakhutdinov. Action recognition using visual attention. In *International Conference on Learning Representations (ICLR) Workshop*, May 2016. [2](#)
- [40] Karen Simonyan, Andrea Vedaldi, and Andrew Zisserman. Deep inside convolutional networks: Visualising image classification models and saliency maps. In *Workshop at International Conference on Learning Representations*, 2014. [2](#)
- [41] Khurram Soomro, Amir Roshan Zamir, and Mubarak Shah. UCF101: A dataset of 101 human actions classes from videos in the wild. *CoRR*, abs/1212.0402, 2012. [2](#), [4](#)
- [42] Alexandros Stergiou, Georgios Kapidis, Grigorios Kalliatakis, Christos Chrysoulas, Ronald Poppe, and Remco C. Veltkamp. Class feature pyramids for video explanation. In *2019 IEEE/CVF International Conference on Computer Vision Workshops, ICCV Workshops 2019, Seoul, Korea (South), October 27-28, 2019*, pages 4255–4264. IEEE, 2019. [2](#)
- [43] Alexandros Stergiou, Georgios Kapidis, Grigorios Kalliatakis, Christos Chrysoulas, Remco C. Veltkamp, and Ronald Poppe. Saliency tubes: Visual explanations for spatio-temporal convolutions. In *2019 IEEE International Conference on Image Processing, ICIP 2019, Taipei, Taiwan, September 22-25, 2019*, pages 1830–1834. IEEE, 2019. [2](#)
- [44] Erico Tjoa and Cuntai Guan. A survey on explainable artificial intelligence (xai): Toward medical xai. *IEEE Transactions on Neural Networks and Learning Systems*, 32(11):4793–4813, 2021. [1](#), [2](#)
- [45] Michalis Vrigkas, Christophoros Nikou, and Ioannis A. Kakadiaris. A review of human activity recognition methods. *Frontiers in Robotics and AI*, 2, 2015. [1](#)
- [46] Haofan Wang, Zifan Wang, Mengnan Du, Fan Yang, Zijian Zhang, Sirui Ding, Piotr Mardziel, and Xia Hu. Score-cam: Score-weighted visual explanations for convolutional neural networks. In *Proceedings of the IEEE/CVF Conference on Computer Vision and Pattern Recognition (CVPR) Workshops*, June 2020. [1](#)
- [47] Huifen Xia and Yongzhao Zhan. A survey on temporal action localization. *IEEE Access*, 8:70477–70487, 2020. [1](#)
- [48] Kelvin Xu, Jimmy Ba, Ryan Kiros, Kyunghyun Cho, Aaron Courville, Ruslan Salakhutdinov, Rich Zemel, and Yoshua Bengio. Show, attend and tell: Neural image caption generation with visual attention. In Francis Bach and David Blei, editors, *Proceedings of the 32nd International Conference on Machine Learning*, volume 37 of *Proceedings of Machine Learning Research*, pages 2048–2057, Lille, France, 07–09 Jul 2015. PMLR. [2](#)
- [49] Guoan Yang, Yong Yang, Zhengzhi Lu, Junjie Yang, Deyang Liu, Chuanbo Zhou, and Zien Fan. Sta-tsn: Spatial-temporal attention temporal segment network for action recognition in video. *PLOS ONE*, 17(3):1–19, 03 2022. [2](#), [5](#)
- [50] Jianming Zhang, Sarah Adel Bargal, Zhe Lin, Jonathan Brandt, Xiaohui Shen, and Stan Sclaroff. Top-down neural attention by excitation backprop. *International Journal of Computer Vision*, 126(10):1084–1102, 2018. [1](#), [2](#)
- [51] Jianming Zhang, Zhe L. Lin, Jonathan Brandt, Xiaohui Shen, and Stan Sclaroff. Top-down neural attention by excitation backprop. In Bastian Leibe, Jiri Matas, Nicu Sebe, and Max Welling, editors, *Computer Vision - ECCV 2016 - 14th European Conference, Amsterdam, The Netherlands, October 11-14, 2016, Proceedings, Part IV*, volume 9908 of *Lecture Notes in Computer Science*, pages 543–559. Springer, 2016. [1](#), [2](#)
- [52] Bolei Zhou, Aditya Khosla, Agata Lapedriza, Aude Oliva, and Antonio Torralba. Learning deep features for discriminative localization. In *Proceedings of the IEEE Conference on Computer Vision and Pattern Recognition (CVPR)*, June 2016. [2](#)
- [53] Yi Zhu, Xinyu Li, Chunhui Liu, Mohammadreza Zolfaghari, Yuanjun Xiong, Chongruo Wu, Zhi Zhang, Joseph Tighe, R. Manmatha, and Mu Li. A comprehensive study of deep video action recognition. *CoRR*, abs/2012.06567, 2020. [1](#), [3](#)